Mixed Fluorinated/Hydrogenated Self-Assembled Monolayer-Protected Gold Nanoparticles: In Silico and In Vitro Behavior

Domenico Marson, Filomena Guida, Maria Şologan, Silvia Boccardo, Paolo Pengo, Fabio Perissinotto, Valentina Iacuzzi, Elena Pellizzoni, Stefano Polizzi, Loredana Casalis, Lucia Pasquato, Sabrina Pacor,* Alessandro Tossi, and Paola Posocco**

Gold nanoparticles (AuNPs) covered with mixtures of immiscible ligands present potentially anisotropic surfaces that can modulate their interactions at complex nano–bio interfaces. Mixed, self-assembled, monolayer (SAM)-protected AuNPs, prepared with incompatible hydrocarbon and fluorocarbon amphiphilic ligands, are used here to probe the molecular basis of surface phase separation and disclose the role of fluorinated ligands on the interaction with lipid model membranes and cells, by integrating in silico and experimental approaches. These results indicate that the presence of fluorinated amphiphilic ligands enhances the membrane binding ability and cellular uptake of gold nanoparticles with respect to those coated only with hydrogenated amphiphilic ligands. For mixed monolayers, computational results suggest that ligand phase separation occurs on the gold surface, and the resulting anisotropy affects the number of contacts and adhesion energies with a membrane bilayer. This reflects in a diverse membrane interaction for NPs with different surface morphologies, as determined by surface plasmon resonance, as well as differential effects on cells, as observed by flow cytometry and confocal microscopy. Overall, limited changes in monolayer features can significantly affect NP surface interfacial properties, which, in turn, affect the interaction of SAM-AuNPs with cellular membranes and subsequent effects on cells.

1. Introduction

Nanomaterials with size scales of few tens of nanometers are ideal platforms to link physicochemical behavior at the nanoscale with targeted biological functions, where each physicochemical property can, in principle, be tuned to engineer for a specific function.

Nanoparticles based on a gold core (AuNPs), covered with a self-assembled monolayer (SAM) of thiolated molecules, are particularly suited for sensing events at the nano–bio interface. Chemical modification of the surface is key for controlling the NP's biocompatibility, biodistribution, site-specific recognition, and immune responses,[1–7] as the chemical functionalities of ligand molecules are chiefly responsible for interface-related properties. Blends of different ligands can therefore be chosen to conveniently functionalize the AuNP surface to have specific characteristics, leading to so-called "mixed" monolayers.[8] Mixed SAM-AuNPs are complex, self-organizing multivalent materials that exhibit structural features to a certain extent analogous to those of biological systems, such as protein surfaces or supramolecular cellular substructures.[9–14]

Furthermore, the spatial organization of the chains in mixed monolayers may strongly affect the particle's overall behavior.[15–17] Several studies on AuNPs protected by patterned ligand arrangements of various types have addressed the role of the nanoscale arrangement of the ligands in mediating cellular

Dr. D. Marson, Dr. F. Guida, Dr. M. Şologan, S. Boccardo, Dr. E. Pellizzoni, Prof. P. Posocco
Department of Engineering and Architecture
University of Trieste
34127 Trieste, Italy
E-mail: paola.posocco@dia.units.it

Dr. F. Guida, V. Iacuzzi, Prof. S. Pacor, Prof. A. Tossi
Department of Life Sciences
University of Trieste
34127 Trieste, Italy
E-mail: pacorsab@units.it

The ORCID identification number(s) for the author(s) of this article can be found under https://doi.org/10.1002/smll.201900323.

Dr. M. Şologan, Dr. P. Pengo, Prof. L. Pasquato
Department of Chemical and Pharmaceutical Sciences and INSTM Trieste Research Unit
University of Trieste
34127 Trieste, Italy
E-mail: lpasquato@units.it

Dr. F. Perissinotto, Dr. L. Casalis
NanoInnovation Laboratory
Elettra-Sincrotrone Trieste S.C.p.A
34149 Basovizza, Italy

Prof. S. Polizzi
Department of Molecular Science and Nanosystems
Ca' Foscari University
30172 Venezia, Italy

Prof. S. Polizzi
Centro di Microscopia Elettronica "G. Stevanato,"
30172 Venezia-Mestre, Italy

interactions and the resulting physiological response.[18] For example, the arrangement of "chemically immiscible" ligands on the gold surface can affect NP cellular uptake mechanism and/or interaction with proteins.[19–26] This may result in different internalization pathways which significantly affect toxicity, as NPs directly translocating into the cytoplasm are less toxic than those in the lysosomal environment, which can generate toxic cations.[27] This was confirmed by experimental and computational investigations,[28] although the limited number of pertinent studies does not provide a clear and unambiguous understanding of the driving forces governing the interaction of patterned AuNPs with biological targets.

In this context, in the past few years, we have focused on increasing phase segregation in SAM-AuNPs by using mixtures of fluorinated (F) and hydrogenated (H) thiolates, exploiting the well-known immiscibility of hydrocarbons and fluorocarbons. Spontaneous phase separation in supramolecular aggregates of F/H amphiphiles[29,30] is well documented for several such systems (e.g., micelles, Langmuir, and Langmuir–Blodgett films), including 2D SAMs on gold surfaces.[31] Furthermore, fluorinated amphiphiles are receiving increasing interest for biological/biomedical applications[32] as they confer useful properties to the materials they are linked to, such as inertness, facilitated cellular uptake, avoidance of protein denaturation, and reduced toxicity.[33–36] Additionally, being NMR active, fluorine nuclei also assist in probing biological interactions[37] and may lead to novel supramolecular contrast agents for bioimaging.[38–40] This calls for a more in-depth investigation on the role of fluorinated ligands in monolayer-protected nanoparticles in modulating interactions with biological environments such as cellular membranes and cells.

To this end, we have recently reported on fluorinated ligands in both homo- and hetero-monolayer-protected gold NPs, including water-soluble AuNPs protected by mixtures of polyethylene glycol–modified H/F amphiphilic thiols (C8TEG and F8PEG, see **Scheme 1**).[41] Electron spin resonance (ESR) studies of these mixed monolayer NPs indicated phase segregation of the two types of ligands in the shell. This is consistent with a plethora of experimental data demonstrating that fluorinated moieties segregate from hydrogenated ones, thus affecting the overall physico-chemical features of mixed assemblies.[29–31,42] In addition, in silico simulations on H/F SAM-AuNPs suggested that phase segregation is sensitive to core size and/or ligand ratio. In particular, while NPs with a 1:1 F8PEG:C8TEG ratio and a core size of 1.6 nm appeared to present completely separated phases, the same ligand ratio but slightly increased core size of 2.2 nm led to alternating C8TEG/F8PEG domains. This could explain the behavior of an ESR probe in the two types of NP.[41]

Core size as well as C8TEG/F8PEG ratio can therefore result in morphological differences, which affect the interfacial area between the two ligands. This could in turn influence the interactions with biological systems since it may alter the NP interface.

We here describe AuNPs prepared with somewhat different ligand composition and core size, and assess how they interact with lipid membranes using both surface plasmon resonance (SPR) and in silico methods. This then allows us to interpret internalization and cytotoxic effects on MEC-1 cells in terms of different putative ligand organizations and how this could affect membrane interaction. The biophysical and biological experimental data consistently show a differential behavior for different mixed SAM-AuNPs, in agreement with the hypothesis that they are protected by monolayers with differing interfacial area and arrangement, also supported by in silico predictions.

2. Results and Discussion

2.1. Synthesis and Characterization of SAM-AuNPs

Two samples of AuNPs protected by blends of F8PEG and C8TEG were prepared following a procedure reported in our previous work[41] and here slightly modified[41,43] (see the Supporting Information). A first batch, named M1-C8T/F8P, is characterized by an average core diameter of 1.6 nm and a C8TEG/F8PEG ratio of 1/1.3 (see **Table 1** and the Supporting Information). A second batch, named M2-C8T/F8P, presents an average core diameter of 1.9 nm and a C8TEG/F8PEG ratio of 1/1.8.

Beside these two types of mixed-monolayer NPs, three homoligand AuNPs (named C8T, C8P, and F8P) were prepared as reference (see Table 1 and the Supporting Information). The mixed-SAM and C8P or F8P homoligand AuNPs could be dissolved in water up to 10 mg mL^{-1}, due to the thick polar polyethylene glycol (PEG) surface layer (see Scheme 1), while C8T AuNPs were difficult to dissolve even at 1 mg mL^{-1}, because of the shallower triethylene glycol (TEG) surface. For this reason, C8T AuNPs were used for molecular simulations but not for experimental investigations.

There are a limited number of experimental techniques able to directly probe the morphology of mixed self-assembled monolayers[18] and, to our knowledge, none are currently available to determine the morphology of mixed ligand nanoparticles protected by thiolates of this size and with such different chemical properties. Scanning tunneling microscopy (STM) is only applicable to relatively short ligands

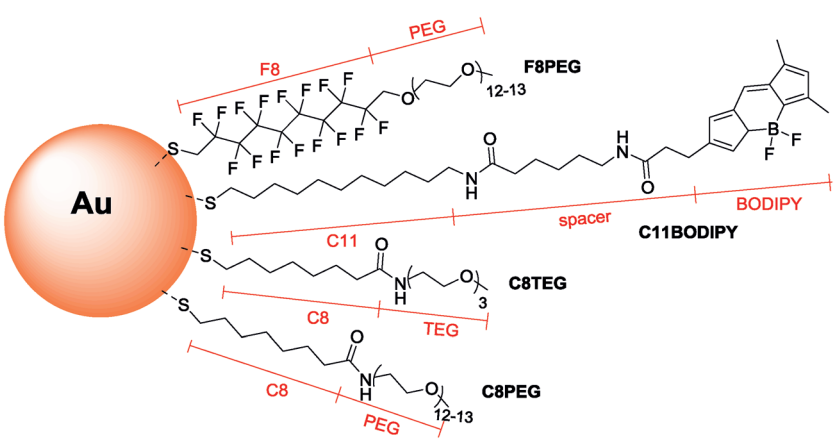

Scheme 1. Structure of thiolated ligands used in this study to pattern the surface of AuNPs.

Table 1. Composition and average size of SAM-AuNPs used in this investigation.

SAM-AuNP	Core diameter[a)] [nm]	NP composition[b,c)]	Ligand ratio C8TEG: F8PEG	NP diameter[d)] [nm]
M1-C8T/F8P	1.6 ± 0.4	$Au_{140}C8TEG_{24}F8PEG_{32}$	42.9: 57.1	6.6 ± 0.1
M2-C8T/F8P	1.9 ± 0.7	$Au_{260}C8TEG_{20}F8PEG_{36}$	35.7: 64.3	6.7 ± 0.2
F8P	2.4 ± 0.7	$Au_{459}F8PEG_{76}$	–	7.6 ± 0.2
C8T	2.0 ± 0.3	$Au_{223}C8TEG_{73}$	–	6.2 ± 0.1
C8P	1.7 ± 0.3	$Au_{201}C8PEG_{69}$	–	7.3 ± 0.1

[a)]From transmission electron microscopy (TEM) measurements; [b)]Calculated from TGA and TEM analysis; [c)]Calculated from thermogravimetric analysis (TGA) and for mixed-monolayers using the ligand ratio determined by ^{1}H NMR on decomposed NPs; [d)]From atomistic simulations, considering both core and ligand shell.

(<14 atoms).[44] NMR could be employed in principle to probe surface domains[45,46] but depends on the availability of signals sensible to changes in the monolayer composition/morphology and suitable for NMR analysis that are lacking. Matrix-assisted laser desorption/ionization mass analysis (MALDI-MS) could also distinguish different surface organizations of immiscible thiolate ligands,[47] but only if they desorb with equal probability,[48] which is not necessarily the case, particularly in presence of fluorinated ligands,[38] as we have also observed.[49] Finally, another alternative, small angle neutron scattering (SANS), is limited to nanoparticle samples with very narrow size dispersity,[50] not achievable for C8TEG/F8PEG-modified AuNPs with our current synthetic methodologies. This left an in silico approach as the only viable method currently available to directly characterize this type of monolayer self-organization, given also it has already been successful in predicting phase segregation of several mixtures of immiscible thiols at molecular level.[41,45,50]

2.2. Nanoparticles Interaction with a Model Membrane

The capacity to bind to a simple model biological membrane composed of only one type of phospholipid was probed using a SPR technique. Zwitterionic 1,2-dioleoyl-*sn*-glycero-3-phosphocholine (DOPC) was chosen as it is commonly used in model membrane experiments.[51–55]

The sensorgrams (**Figure 1**) confirmed that both M1- and M2-C8T/F8P AuNPs were capable of binding to the DOPC membrane. In both cases, they showed a fast binding kinetics, and the concentration-dependent increase in "resonance units" (RU) suggested a good adhesion capacity to the membrane surface. The calculated affinity constant (K_D) estimated from the binding curves (Figure 1B,D), however, indicated that M2-C8T/F8P AuNPs had a fourfold higher affinity for the membrane ($K_D = 80 \times 10^{-6}$ M) than M1-C8T/F8P AuNPs ($K_D = 330 \times 10^{-6}$ M). We also tested the affinity of the C8P and F8P homoligand AuNPs using the same setup. Both of these exhibited a good binding capacity to the DOPC large unilamellar vesicle (LUV) surface, the RU increasing in a concentration-dependent manner similar to that of the mixed-ligand NPs (Figure S1A–D, Supporting Information). F8P AuNPs showed a higher affinity than C8P AuNPs ($K_D = 60 \times 10^{-6}$ and 118×10^{-6} M, respectively).

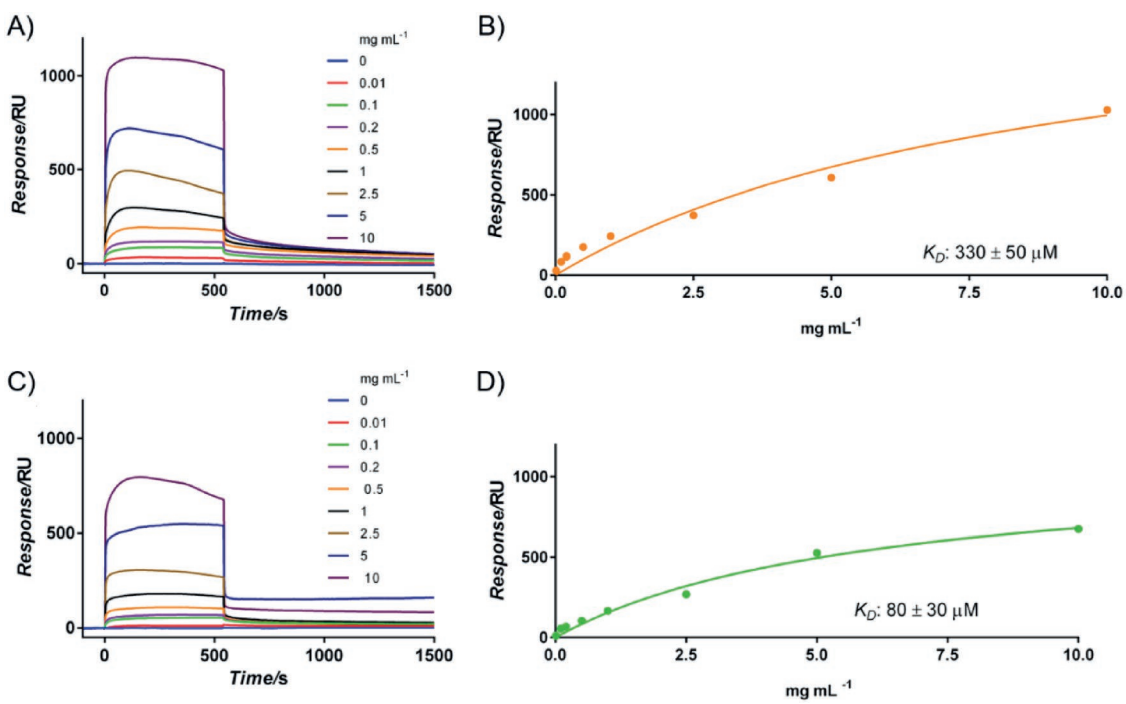

Figure 1. A,C) Binding sensorgrams and B,D) binding curves for A,B) M1- and C,D) M2-C8T/F8P AuNPs. Sensorgrams were obtained flowing SAM-AuNPs at increasing concentrations (as shown) over DOPC LUVs immobilized on an L1 sensor chip. Binding curves were fitted using the "Affinity-Steady State" mathematical model. Shown is one experiment out of five different evaluations with very similar results.

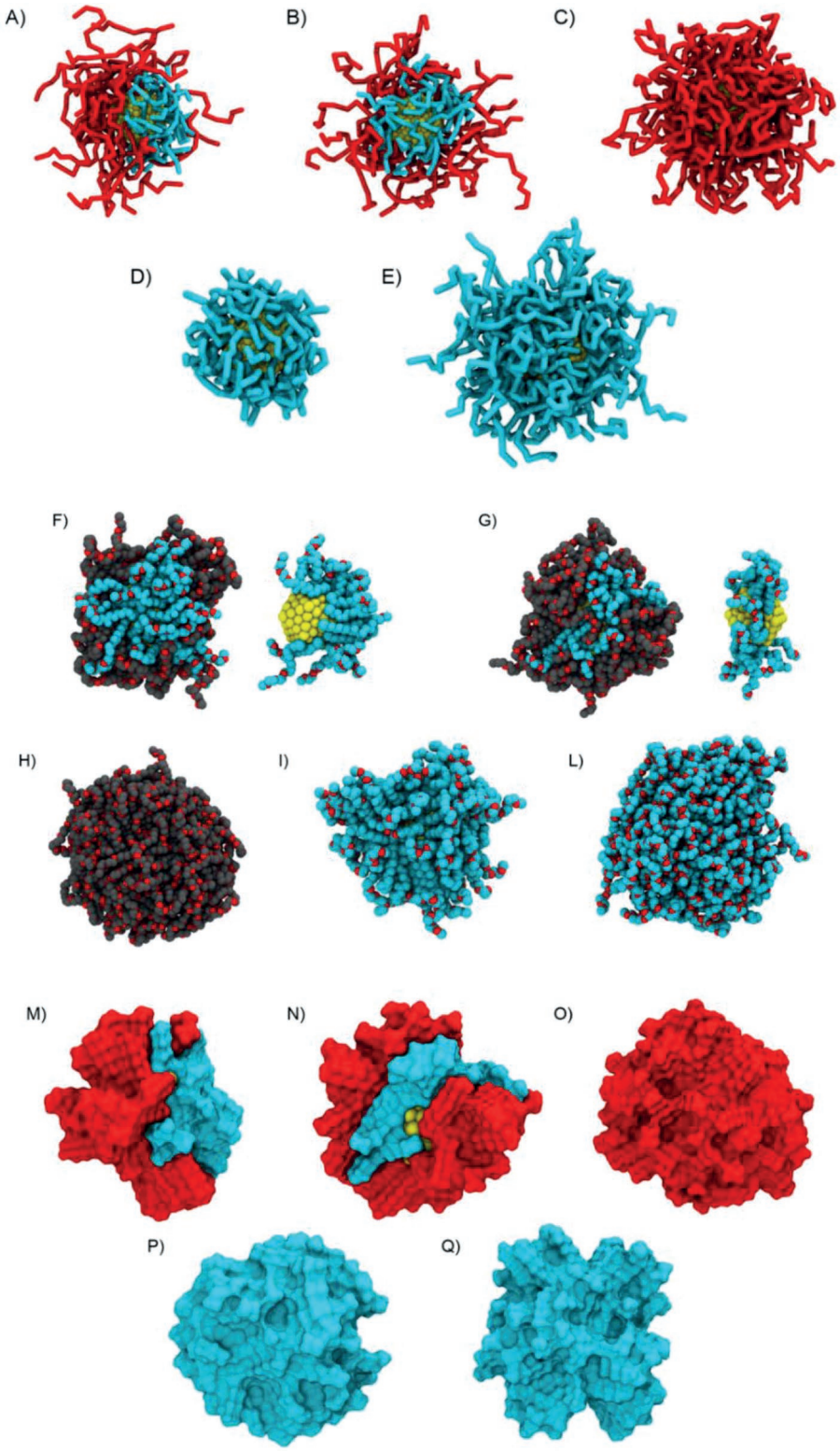

Figure 2. Self-assembled monolayer organization of SAM-AuNPs as obtained from A–E) CG and F–L) AA-MD calculations in explicit water. A,F) M1-C8T/F8P, B,G) M2-C8T/F8P, C,H) F8P, D,I) C8T, and E,L) C8P AuNPs. A–E) Color code: red, F8PEG-thiolates; cyan, C8TEG/C8PEG-thiolates; yellow, gold core. F–L) Color code: F8PEG and C8TEG/C8PEG carbon atoms are in grey and cyan, respectively, while oxygen atoms are in red. Water and inorganic ions are not shown for the sake of clarity. Only the hydrophobic portion of each thiolate (i.e., C8 part of C8TEG or C8PEG, and F8 part of F8PEG, see Scheme 1) is depicted as red and cyan molecular surface, respectively, to emphasize ligand bundling and arrangement in the inner part of the monolayer. M) M1-C8T/F8P, N) M2-C8T/F8P, O) F8P, P) C8T, and Q) C8P AuNP. Nanoparticles are not drawn to scale.

We then investigated whether the marked difference in affinity constant of the two mixed systems could be rationalized using theoretical calculations, which can provide specific molecular insights into how the monolayer organization could affect the ability to bind DOPC bilayers.

Using the physical and chemical characteristics of the synthesized AuNPs (see Table 1), we ran coarse-grained (CG) simulations to characterize the behavior of the ligands in the homo layer NPs, and self-sorting of the C8TEG/F8PEG ligands, initially inserted at random onto the gold surface, in the mixed layer NPs. This showed that the C8TEG and F8PEG chains self-organized in the M1 and M2 NPs in a manner that led to different surface patterns. In M1-C8T/F8P the ligands seemed to separate into two distinct domains, reminiscent of what has been termed a "Janus-like" morphology (**Figure 2**A). Conversely, M2-C8T/F8P displayed an F8PEG/C8TEG/F8PEG domain arrangement, conforming more to the so-called "stripe-like" morphology (Figure 2B).[18] This is entirely in line with the conceptual framework described in the "Introduction" on how parameters such as core size and C8TEG/F8PEG ratio affect surface morphology.[41] The final structures can be compared to those of the homoligand AuNPs in Figure 2C–E.

A more detailed picture of ligand conformation and monolayer properties at the molecular level required switching to all-atom molecular dynamics (AA-MD) simulations starting from the solvated CG structures (see Figure 2F–L). Snapshots of the equilibrated C8P and F8P AuNP structures clearly showed the fluid nature of the outer shell of the monolayers with the longer PEGylated portion of the thiolates, and no visual indication of crystallization, whereas this is evident for the C8T AuNPs, with the shorter TEGylated portion. Considering only the inner, hydrophobic part of the monolayer, a degree of ordering is observed in all NPs, with evidence of ligand bundling involving the fluorinated (F8) or hydrogenated (C8) portions of the ligands (see Scheme 1 and Figure 2M–Q). More detail on the monolayer structure and properties is provided in the Supporting Information.

The NPs obtained from the CG simulations were then placed in an aqueous phase above a DOPC bilayer, and unconstrained Martini MD simulations were carried out. All NPs approach the membrane from solution and partition into the water–lipid interface (Figure S3, Supporting Information), rapidly reaching and then maintaining an equilibrium distance value, suggesting that binding is stable over time (Figure S4, Supporting Information). This is consistent with the binding capacity and fast kinetics evidenced by SPR experiments. Spontaneous insertion of NPs into, or translocation through, the DOPC membrane was not observed in the 10 μs timescale of unbiased MD simulations, although it may occur subsequently (see the following sections).

NP-DOPC adhesion (ΔG_{adh}) was quantified by free energy calculations using an umbrella sampling technique (see **Table 2** and Figure S5 in the Supporting Information). M1- and M2-C8T/F8P both showed a lower affinity for the DOPC layer (less negative ΔG_{adh}), with respect to PEG homoligand NPs, and this is not simply due to the different number of ligands.[56]

The surface morphology also appeared to play an important role in surface interactions as M1-C8T/F8P has a significantly lower interaction energy (–28.6 kcal mol^{-1}) than M2-C8T/F8P (–38.9 kcal mol^{-1}), nicely matching the trend emerging from the SPR analysis. The separation of ligands into nanoscale domains also decreased the number of ligands residing at the water–lipid interface N_C from ≈30 in homoligand NPs to only ≈21–25 for mixed ligand NPs, and in both cases the contacts almost all involve F8PEG chains.

Table 2. Computational analysis of adhesion energy and contacts at the interface between SAM-AuNPs and a DOPC membrane.

SAM-AuNP	ΔG_{adh}[a] [kcal mol^{-1}]	N_C[b]	Contacts	
			Hydrophilic[d] [%]	Hydrophobic[e] [%]
M1-C8T/F8P	–28.6 ± 1.5	21 ± 2 (0/21)[c]	59	41
M2-C8T/F8P	–38.9 ± 1.0	25 ± 1 (3/22)[c]	63	37
F8P	–51.0 ± 1.2	32 ± 2	73	27
C8T	–20.7 ± 0.7	28 ± 2	53	47
C8P	–44.1 ± 0.8	31 ± 2	72	28

SAM-AuNP/DOPC interaction assessed in terms of; [a]Adhesion energy (kcal mol^{-1}); [b]Total number of NP ligands in contact with the lipid bilayer (distance < 0.6 nm between ligand and lipid beads in CG simulations); [c]Contribution to the total number of contacts NC pertaining to C8TEG and F8PEG chains, respectively; [d]Relative number of NP–DOPC contacts involving hydrophilic ligand moieties (PEG, TEG); [e]Relative number of NP–DOPC contacts involving hydrophobic ligand moieties (C8, F8).

The immiscibility and different steric hindrance of ligands in the mixed systems affect interchain association, and result in the presence of interfaces between ligands, which may affect the capacity of ligands to adapt in a responsive manner and reduce the average number of chains involved in membrane binding, apparently more so for M1- than M2-C8T/F8P AuNPs. This is in line with previous observations that the behavior of nanometer-scale structures in interfacial-related phenomena is more dependent on the surface morphology than on the ligand composition and their physico-chemical properties.[17]

One might argue that the more favorable ΔG_{adh} of M2-C8T/F8P with respect to M1-C8T/F8P is simply due to the additional N_C (see Table 2) without a significant role of the different morphologies. Should this be the case, however, one would expect that the ΔG_{adh}^{M2} should be comparable to ΔG_{adh}^{M1} plus the contributions of the added 3 H and 1 F contacts. These may be obtained, to a first approximation, as $\Delta G_{adh}^{C8T}/28$ and $\Delta G_{adh}^{M1}/22$ (which approach the membrane exposing only F ligands), respectively. ΔG_{adh}^{M2} estimated this way is –32.2 kcal mol^{-1}, which is significantly less favorable than that obtained by the umbrella sampling calculations (–38.9 kcal mol^{-1}), suggesting a significant further contribution to the interaction from the morphology.

In addition, while for M1-C8T/F8P the reduced interaction energy with respect to F8P (–28.6 vs –51.0 kcal mol^{-1}, respectively) is accompanied by an increased dissociation constant as determined by SPR (≈330 × 10^{-6} and ≈60 × 10^{-6} M, respectively), for M2-C8T/F8P the ΔG_{adh} decreases from –51.0 to –38.9 kcal mol^{-1}, but the dissociation constants are quite similar (≈60 × 10^{-6} and ≈80 × 10^{-6} M, respectively). This indicates that there is an added component to membrane binding that is not picked up in the time scale of the MD simulation, possibly a further penetration into the lipid bilayer

occurring in the timescale of the SPR experiment, in line with cellular internalization observations (see the following sections).

The homoligand F8P AuNPs exhibit the most negative ΔG_{adh} value (strongest interaction) with a favorable contribution of long PEG chains on adsorption properties, in agreement with SPR data. The number of hydrophilic and hydrophobic contacts with DOPC (see Table 2) is remarkably similar for F8P and C8P, so the more negative ΔG_{adh} of F8P is due to the increased hydrophobic effect of the fluorinated moiety. Thus, while most of the NP-DOPC contacts are to be attributed to hydrophilic PEG unit contacts, hydrophobic contributions (≈30%) stemming from C8/F8 moiety contacts are not negligible, thanks to ligand flexibility.

Overall, it would appear that inherent ligand features and monolayer organization that are buried out in aqueous solution (where NPs behave similarly; see Table S1 in the Supporting Information) start to play a major role at the nano–bio interface.

2.3. Interaction with Complex Model Membranes

We then moved toward more complex membrane models, in an attempt to reduce the gap between single-component synthetic bilayers and real multicomponent cell membranes, by building a multicomponent raft-like membrane model. Membrane rafts are thought to be implicated in key cellular processes, such as signaling, endocytosis, and adhesion.[57–59]

A ternary mixture of DOPC, sphingomyelin (SM), and cholesterol (Ch) was selected as a representative system, with cholesterol levels resembling those in biological membranes (≈25% mol). Atomic force microscopy (AFM) images of a supported DOPC/SM/Ch bilayer were obtained (**Figure 3**) and used to guide the construction of a multicomponent molecular model resembling the experimental domain organization but in a 2D periodic boundary condition[60] (see the Supporting Information for details).

Regardless of their SAM chemistry, all the NPs preferred to contact the membrane within the fluid DOPC-rich domain (L_d) (Figure 3; Figure S6, Supporting Information). Preferential adsorption on the disordered phase may be driven by the lower bending modulus of the L_d phase, which enhances the number of favorable contacts between flexible ligands and lipids as seen very recently by Liang and co-workers for other ligand coated nanoparticles.[61] The main features of the NP/membrane interface were preserved with respect to a simple DOPC membrane (see Table S2 in the Supporting Information) and the two mixed systems still behaved differently; only the values of N_C decreased slightly (by 2–3 contacts) as compared with pure DOPC membrane. Ch molecules can substantially influence membrane physical properties such as fluidity,[62,63] so that the reduction in the number of ligands participating the binding may be attributed to the ordering and condensing effect of Ch, and to the increased local rigidity of the DOPC phase, due to residual Ch.

This new set of simulations provides some potentially important indications: i) the fundamental role of membrane fluidity along with ligand flexibility in tailoring the nano–bio interface; ii) the preference of this type of SAM-AuNP in general to interact with the L_d phase of complex membranes rather than with the L_o raft-like phase, and iii) that NP surface organization is as relevant for interaction with more complex synthetic membranes as for simple homogeneous ones.

2.4. Effect of Nanoparticles on Host Cells: Cytotoxicity Evaluation

The biological effect of SAM-AuNPs was assessed by exposing a human B lymphocyte–derived cell line (MEC-1) to concentrations of up to 1 mg mL^{-1} of the different NPs, in complete medium, for 24 h, and then determining metabolic cytotoxicity. Results obtained with MEC-1, which grow in suspension, indicate that some cytotoxicity is limited to M1-C8T/F8P AuNPs, which reduce viability by 10–20% (**Figure 4**). Overall, none of the NPs caused a statistically significant reduction of viability in comparison to untreated controls. Furthermore, comparable results were obtained with monocyte-derived U937 (not shown) as well as epithelial-derived A459 cell lines (see Figure S7 in the Supporting Information).

Moreover, the integrity of the plasma membrane was assessed by determining its permeabilization to propidium iodide (PI).

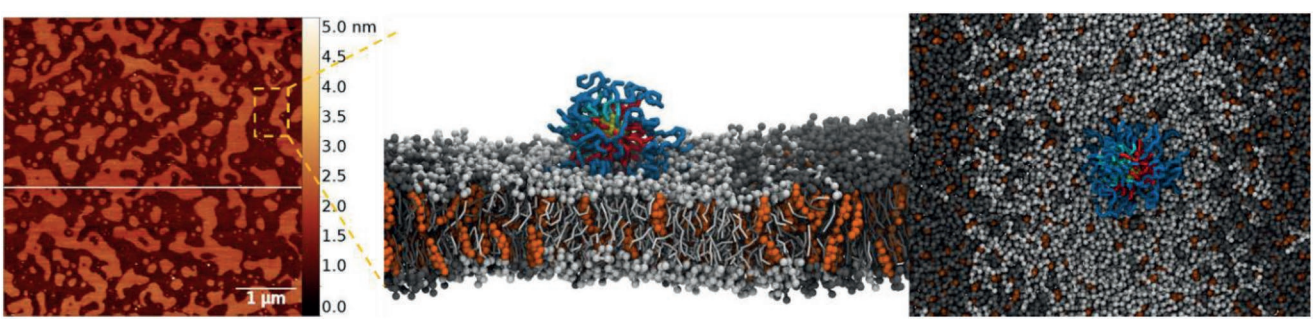

Figure 3. AFM image of supported DOPC/SM/Ch bilayer and equilibrated simulation snapshot of M1-C8T/F8P AuNP interacting with the same ternary mixture. Left panel: AFM images (scan size 5 × 5 nm^2) in noncontact mode of a supported membrane prepared from a DOPC/SM/Ch mixture with scale bar 1 µm. Lateral view (middle panel) and top view (right panel) of an M1-C8T/F8P AuNP adhered to the DOPC/SM/Ch bilayer. The hydrophilic PEG component of the ligands is colored in blue, while the hydrophobic F8 and C8 moieties are highlighted in red and cyan, respectively. The gold core is shown in yellow. DOPC headgroups and tails appear as light gray spheres and sticks, respectively, while for SM they are in dark gray. Ch molecules are highlighted as orange spheres. Water and inorganic ions are not shown for clarity.

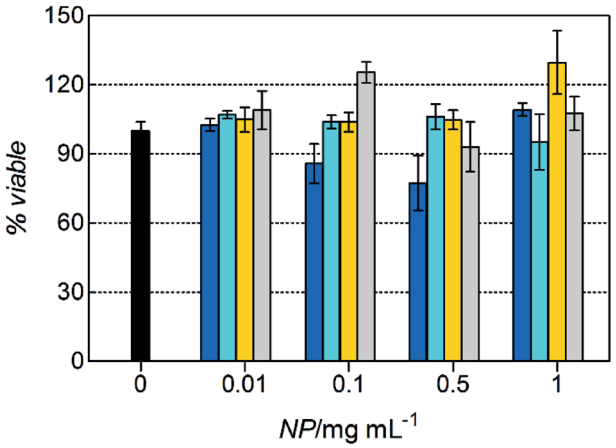

Figure 4. Cytotoxicity of MEC-1 cells exposed to different SAM-AuNPs. Cell viability was evaluated by the MTT assay, after 24 h exposure to NPs at the reported concentrations. Data are expressed as mean ± SEM of the measured O.D., for at least three independent experiments performed in triplicate. Color legend: M1-C8T/F8P AuNPs, blue; M2-C8T/F8P AuNPs, turquoise; F8P AuNPs, yellow; and C8P AuNPs, gray.

No membrane permeabilization was observed even for the highest concentration (1 mg mL^{-1}) and up to 60 min of exposure (PI positive cells were ≈5%, comparable to controls), suggesting that no necrotic damage was induced by NPs.

We then used JC-1[64] as a probe of apoptotic damage to mitochondrial functionality.[65] We ran untreated control with functional mitochondria (**Figure 5**A, orange fluorescence) in parallel to cells treated with the known depolarizing agent carbonyl cyanide 3-chlorophenylhydrazone (CCCP) showing mainly inactive mitochondria (Figure 5B, green fluorescence). When MEC-1 cells were treated with M2-C8T/F8P (Figure 5C) or M1-C8T/F8P (Figure 5D) AuNPs, no significant decrease in orange fluorescence was observed by either confocal microscopy or flow cytometric analyses. In particular, the mean fluorescent intensity (MFI) signals recorded by flow cytometry (Figure 5E) are comparable to the values for functional mitochondria of untreated control cells.

Taken together, experiments performed on model cell lines indicate that M1- and M2-C8T/F8P AuNPs are both well tolerated by host cells, as neither the plasma membrane nor mitochondria is damaged to any significant extent after exposure to 1 mg mL^{-1} NP in either buffer (up to 60 min) or complete medium (24 h). These results prompted us to explore the possibility that NPs could interact with cells and then be internalized, without damaging their membrane.

2.5. Interaction with Cells and Cellular Internalization

NPs tagged with a boron dipyrromethene (BODIPY) fluorophore, (see Scheme 1) were prepared (see Table S3 in the Supporting Information) and fully characterized (see the Supporting Information). These NPs were used to assess the capacity of the different NPs to associate with the surface of eukaryotic cells and to then be internalized. The fact that cells became fluorescent when incubated with all types of NP suggested that these associated with the cellular surface, although the intensity of the MFI signal varied significantly among the different NPs employed. The fluorescence data can only be interpreted qualitatively for two reasons. The first is that the labeling process, which was carried out by ligand exchange (see the Supporting Information), varied significantly from one NP to the other, leading to a different BODIPY loading. While M1-C8T/F8P AuNPs and homoligand NPs were tagged with ≈2 BODIPY/NP, M2-C8T/F8P AuNPs in fact had ≈6. The second reason is that the F8 moiety seems to quench BODIPY fluorescence more than the C8, and in a surface pattern-dependent manner (see Table S2 in the Supporting Information). This means that

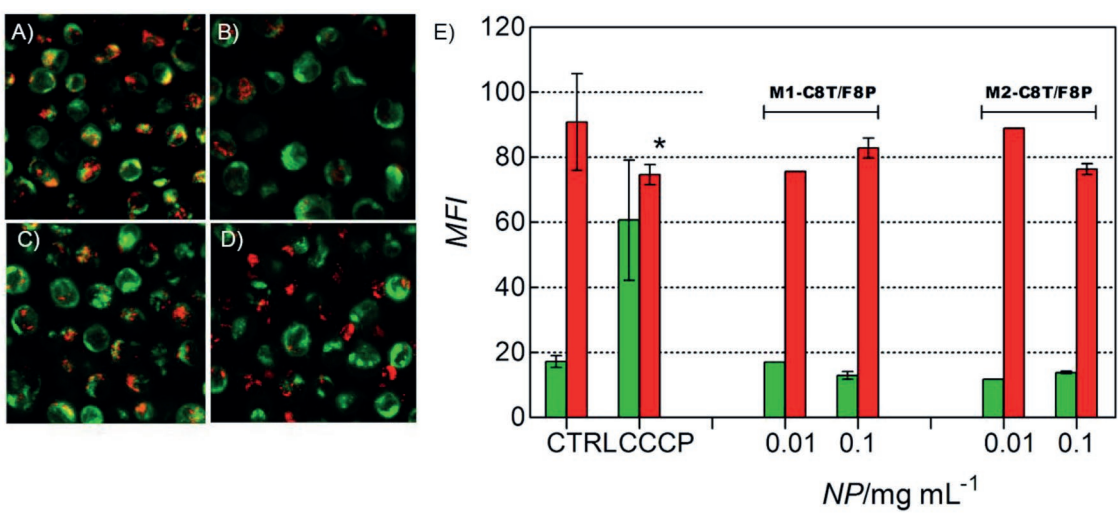

Figure 5. Effect of SAM-AuNP on mitochondrial inner transmembrane potential of MEC-1 cells. Cells were stained with JC-1 probe and treated for 60 min with M1- and M2-C8T/F8P AuNPs. (Left panel) Confocal images of A) untreated control cells (CTRL), B) CCCP treated cells (positive control), C) M2-C8T/F8P AuNPs, and D) M1-C8T/F8P AuNP-treated cells (both at 0.1 mg mL^{-1}). E) MFI values of MEC-1 cells obtained by flow cytometric analysis, where green columns represent green fluorescence (JC-1 monomeric) and red columns represent orange fluorescence (JC-1 aggregated). Data for M1- and M2-C8T/F8P AuNPs are labeled above the corresponding columns. Results are shown as mean ± SEM of three experiments. *$p < 0.05$ versus CTRL, *t*-test.

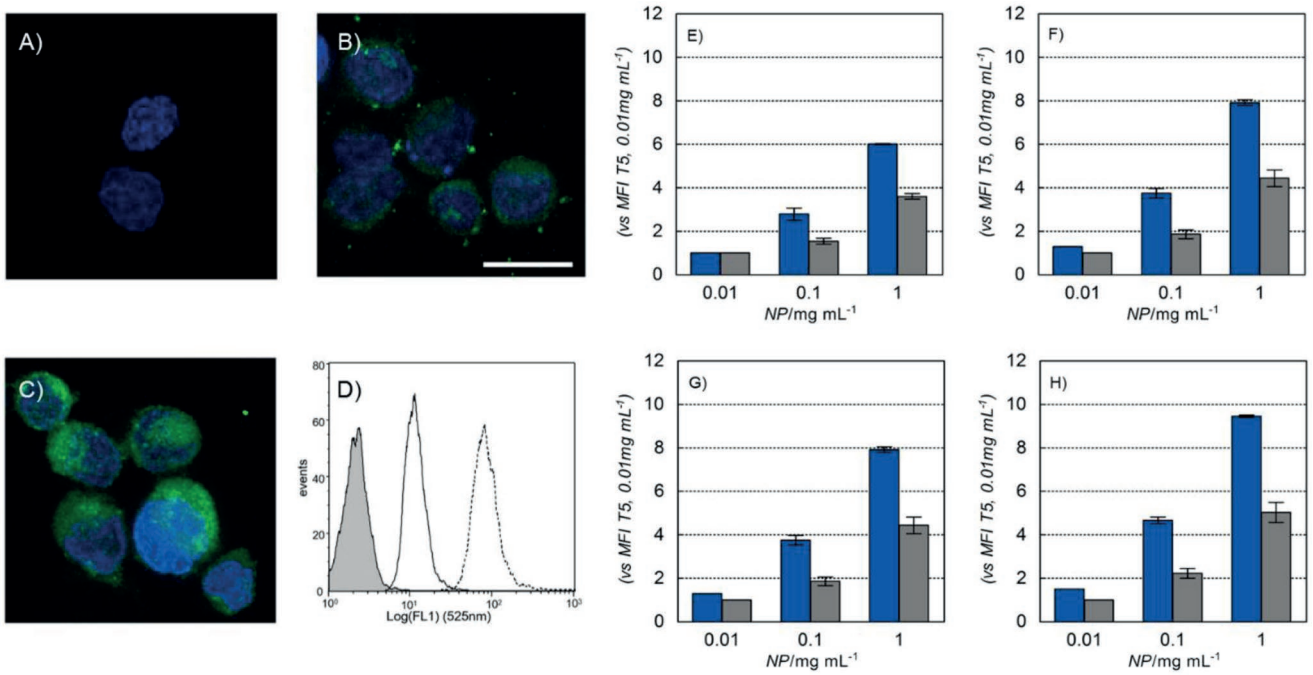

Figure 6. Confocal microscopy and flow cytometry of cells treated with mixed-ligand, BODIPY-tagged SAM-AuNPs. Confocal images of A) control MEC-1 cells, B) cells treated with 1 mg mL^{-1} M1-C8T/F8P/BODIPY AuNPs, and C) cells treated with 0.1 mg mL^{-1} M2-C8T/F8P/BODIPY AuNPs, for 60 min prior to counterstaining nuclei with Hoechst dye. D) Flow cytometric monoparametric overlay plot of green fluorescence emitted from untreated (gray peak) and cells treated with 1 mg mL^{-1} M1-C8T/F8P/BODIPY AuNPs (——) and 0.1 mg mL^{-1} M2-C8T/F8P/BODIPY AuNPs (-----). Cells were exposed for 60 min with M1- and M2-C8T/F8P/BODIPY AuNPs at the reported concentrations. Data for E) 5 min, F) 15 min, G) 30 min, or H) 60 min with M1- (gray) or M2-C8T/F8P/BODIPY (blue) AuNPs. Values are normalized to the lowest NP concentration (0.01 mg mL^{-1}) at the shortest time (5 min) and are the mean ± SEM of repeated experiments.

the fluorescence of M2-C8T/F8P/BODIPY AuNPs was intrinsically higher than that of M1-C8T/F8P/BODIPY AuNPs, and that of C8P/BODIPY AuNPs was intrinsically higher than that of F8P/BODIPY AuNPs, at the same concentrations.

The confocal analysis (**Figure 6**) clearly showed that both M1- and M2-C8T/F8P/BODIPY AuNPs crossed the plasma membrane to reach the cytoplasm, while they did not appear to localize in the nuclear compartment. Furthermore, even taking the difference of BODIPY loading and quenching into account, by using M1-C8T/F8P/BODIPY AuNPs at a concentration ten times higher than M2-C8T/F8P/BODIPY AuNPs (see Table S2 in the Supporting Information), the fluorescence of treated cells appeared less intense. This was confirmed also by flow cytometric analysis (Figure 6D).

The effects of NP concentration and exposure time on the interaction of M1- and M2-C8T/F8P/BODIPY AuNPs with MEC-1 cells, as determined by flow cytometry, are shown in Figure 6E–H and in Figure S8 (Supporting Information). There is clearly a difference in the MFI signal of NP-treated cells, due to the different intrinsic fluorescence of the particles, so that M1-C8T/F8P/BODIPY AuNPs emit at about tenfold lower intensity with respect to M2-C8T/F8P/BODIPY AuNPs (see Figure S8 in the Supporting Information). To take these differences into account, the MFI values of BODIPY-labeled NP were normalized to those at the lowest concentration used for each at the shortest incubation time (i.e., 0.01 mg mL^{-1} for 5 min), allowing a comparison of fold increase in fluorescence with time, independently of the different basal signals. These data indicate a rapid interaction of both types of NPs with the cells, which is most evident for M2-C8T/F8P/BODIPY AuNPs, and that both are retained by the cells, as the fluorescence signal persists after extensive washing. This is consistent with the internalization of the NPs as observed by confocal microscopy (Figure 6A–C). We conclude that both types of mixed SAM-AuNPs interact with, and are internalized into, MEC-1 cells in a time-, concentration-, and morphology-dependent manner.

The same analysis was then extended to BODIPY-labeled homoligand NPs (**Figure 7**). Homo- and mixed SAM-AuNPs were compared at 1 mg mL^{-1} concentration, for 15–60 min exposure of MEC-1 cells, normalizing as explained above. Again, it is evident that NP adhesion to the cell membrane increases in a time-dependent manner. Overall, M1-C8T/F8P/BODIPY showed least internalization with respect to other systems, in line with a lower membrane interaction, as indicated by both SPR results and computational analyses.

3. Conclusion

We explored the effect of fluorinated and hydrogenated amphiphiles in homoligand and mixed SAM-protected AuNPs on NP interactions with lipid bilayers and cells. SPR experiments used to probe NP–lipid interactions showed an enhanced binding for completely fluorinated NPs, and a significant difference in the binding capacity of two mixed systems. AA and CG MD

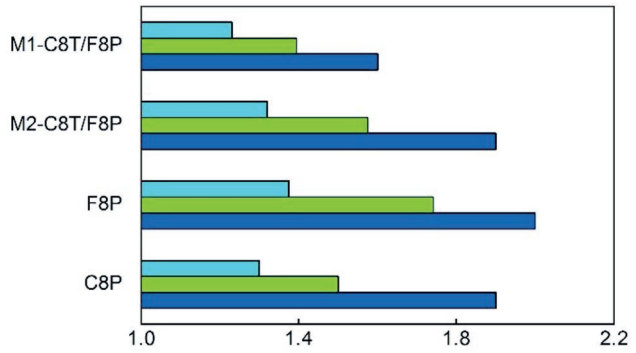

Figure 7. Fold increase of florescence with exposure time for cells treated with BODIPY-tagged SAM-AuNPs of different type. The fluorescence increase is referred to the MFI values obtained in flow cytometry experiments at 15 (■), 30 (■), and 60 (■) min exposure to NP as compared to values after 5 min exposure, for MEC-1 cells incubated with 1 mg mL^{-1} NPs at 37 °C in the presence of PBS buffer.

calculations, performed in conditions that closely resembled those in SPR experiments, provided a molecular basis of factors shaping this differential interaction, and in particular the role of ligand separation into distinct surface morphologies. This also affected how the NP behaved in in vitro cytotoxicity and internalization assays with a leukocyte cell line (3-(4,5-dimethylthiazol-2-yl)-2,5-diphenyl tetrazolium bromide (MTT), flow cytometry, and confocal microscopy).

We consistently observed a dissimilar behavior of the two mixed-monolayer AuNPs, which may be rationalized by assuming a difference in the C8TEG–F8PEG ligand surface organization and domain interfaces, which in turn affects the number, kind, and strength of contacts that occur at the membrane surface, and is consistent with the different time- and concentration-dependent effects at a cellular level.

This study demonstrates that even relatively small differences in the monolayer characteristics of mixed SAM-AuNPs can lead to quantifiable differences in their interaction with biological membranes, suggesting that it can be used to rationally engineer surface properties. For example, modifying the ligand ratio to drive the surface organization in patches or elongated domains of different size is expected to expand the diversity of the biological outcomes since the interfacial features of such nanoparticles are likely distinct from those considered here. Overall, this family of nanoparticles exhibits characteristics well suited for intracellular delivery, so it opens the possibility of tuning the surface properties to direct the internalization and localization processes for diagnostic or drug-delivery purposes. They could also provide novel convenient tools for experimental studies based on membrane sensing or probing the interaction with cellular substructures of increasing complexity. Such studies will be the subject of future work.

4. Experimental Section

Nanoparticle Synthesis and Characterization: M1- and M2-C8T/F8P AuNPs were obtained by direct synthesis using a blend of sodium C8TEG and F8PEG thiolates following a modified procedure reported previously[41,43] and described in the Supporting Information together with a detailed report of preparation and full characterization of the other homoligand NPs.

NPs were labeled with a fluorescent ligand in order to monitor cell interaction and internalization processes by confocal fluorescence microscopy and flow cytometry. For this, a BODIPY FL-X functionalized thiol was used (Scheme 1). The fluorescent units were introduced in the monolayer by place exchange. The general procedure for the preparation of labeled NPs, as well as the synthesis of the thiol containing the dye, are reported in the Supporting Information. It is worth noting that the protocol envisaged introducing only a few BODIPY per NP, in order to minimize the impact of fluorescent ligand on the NP surface–assembled monolayer properties. However, it was not possible to control this precisely. The degree of substitution was established by decomposing the NPs and assessing the amount of dye in solution by means of UV–vis or fluorescent spectroscopy, and the resulting compositions are reported in Table S3 (Supporting Information).

Surface Plasmon Resonance: Interaction studies between NPs and model membranes were carried out using a Biacore ×100 instrument (GE Lifesciences) immobilizing integral liposomes on an L1 sensor chip surface. The L1 sensor chip consists of a thin gold film covered by a carboxymethyl dextran matrix to which lipophilic residues (alkyl chains) have been covalently attached to capture liposomes.[66,67]

Surface Plasmon Resonance—Liposomes Preparation: LUVs were prepared using DOPC. Dry lipids were dissolved in 2:1 v/v chloroform/methanol in a 5 mL round-bottom flask and the solvent was removed under nitrogen and then under vacuum. The dry lipid cake (5×10^{-3} M phospholipid) was hydrated in phosphate-buffered saline (PBS) by spinning the flask at room temperature for 1 h. The resulting suspensions were then subjected to several freeze–thaw cycles prior to extrusion through polycarbonate filters with 100 nm pores using a Mini-Extruder kit (Avanti Polar Lipids, Inc.). The extruded unilamellar LUVs were then diluted to result in $\approx 1 \times 10^{-3}$ M phospholipid in PBS, and confirmed to be ≈100 nm in size by dynamic light scattering (DLS) using a Zetasizer Nano series (Malvern Panalytical Ltd).

Surface Plasmon Resonance—Liposome Capture on the L1 Sensor Chip: The DOPC LUV suspension ($\approx 1 \times 10^{-3}$ M phospholipid) was injected three times onto the chip surface for 10 min with a flow rate of 5 µL min^{-1}. About 9000 RU maximum was reached for all binding experiments, and each of the two channels in the flow cells was used for separate experiments. Subsequently a 50×10^{-3} M sodium hydroxide solution was injected (30 µL min^{-1} for 30 s) to remove loosely bound liposomes. Bovine serum albumin at a concentration of 0.1 mg mL^{-1} was then injected at 5 µL min^{-1} for 60 s to saturate unmasked lipophilic groups on the chip and so prevent nonspecific binding of the NPs. In any case, only a very small increase in the signal was observed (typically < 60 RU), confirming that coverage of the surface with liposomes was effective. The procedure used does not result in liposome fusion on the chip surface.[67]

Surface Plasmon Resonance—Binding Analysis: To determine the binding of NPs with the liposomes, solutions with increasing NP concentrations (from 0.01 to 10 mg mL^{-1}) were injected in succession, at a constant flow rate of 10 µL min^{-1} for a contact time of 540 s, followed by a dissociation time (washing) of 1200 s with PBS running buffer. Binding of the NPs to the LUV resulted in a local variation of the refractive index, leading to altered resonance properties that allow real-time monitoring of the interaction. This was reported as a variation in RU, so that 1 RU ≡ 1 pg of matter binding per mm^2 of surface.[68] Sensorgrams for each condition were obtained using BIAevaluation software v 1.1 and then elaborated using GraphPad v 6.04.

At the end of each run, the flow cell was regenerated with isopropanol and NaOH to remove phospholipids, before being treated with fresh LUV suspension (only a max of three regenerations was used). Each experiment was repeated five times with a given type of NP. The best fit for binding curves was obtained with the "Affinity-Steady State" mathematical model in the BiaEvaluation software, from which it was possible to obtain an equilibrium dissociation constant K_D.

Computational Models and Details: The spontaneous organization of the monolayers was determined by adopting a coarse-grained

computational procedure developed previously by us for NP functionalized with mixtures of C8TEG and F8PEG.[41] These NP structures were then mapped back to the all-atom configurations, and the monolayers were equilibrated in explicit water and physiological concentration of inorganic ions (Na^+ and Cl^-) at ambient temperature. Atomistic simulations were performed using the AMBER 14 suite of this software,[69] employing the gaff2 forcefield.[70,71]

In describing the interaction event of NP with model membranes, this study was returned to a coarse-grained resolution and employed MARTINI forcefield[72] and GROMACS 2016.1 as the simulation platform.[73–78] This allowed to model larger systems for the longer timeframes needed to study the phenomena involved at the nano–bio interface. Unbiased (e.g., without constrains) ≈10 µs MD simulations placing the NPs in the water phase ≈8–9 nm away from the bilayer surface were carried out to investigate NP–lipid bilayer adhesion and interaction with time. Different initial orientations (relative to the C8/F8 interface) were explored for the M1- and M2-C8T/F8P. Simulations were carried out in explicit solvent and in periodic boundary conditions, with box dimensions such as the minimum-image convention being maintained. Details on the parameterization and simulation protocols can be found in the Supporting Information.

The energy involved in membrane binding was quantified using Umbrella Sampling calculations with the pull code available in GROMACS, coupled with the weighed histogram analysis method (WHAM).[79] For details, refer to Supporting Information.

GROMACS and AMBER tools, VMD,[80] insane.py[81] and in-house python scripts were used to build the systems, visualize the trajectory and make all the calculations and images reported in this paper. Where the code was available, computations were performed on graphics processing units (GPUs).

Cell Lines Used: The human MEC-1 cell line (kindly provided by Dr. P. Macor of the Department of Life Sciences, University of Trieste) was cultured in Roswell Park Memorial Institute (RPMI) 1640 medium supplemented with 2×10^{-3} M L-glutamine, 100 U mL^{-1} penicillin, 100 µg mL^{-1} streptomycin, and 10% fetal bovine serum (FBS) (complete medium) and was subcultured two/three times a week, for not more than 20 passages. This cell line was used for all in vitro assays described below.

MTT Metabolic Cytotoxicity Assay: The colorimetric MTT assay was performed, as previously described.[82,83] Briefly, 10^5 cells per well were treated with 0.01–1 mg mL^{-1} of a tested NP. At the end of 24 h exposure time, the NP-containing medium was removed; culture plates were centrifuged, washed twice with PBS; and each cell containing well was filled with fresh medium for the assay in order to avoid the known problem of a specific interference with the development of the MTT assay;[84] 20 µL of MTT solution (5 mg mL^{-1}) was added to each well for 4 h incubation at 37 °C. The converted MTT dye was solubilized with acidic isopropanol (0.04 N HCl in absolute isopropanol). Absorbance was measured at 540 and 630 nm using an automated microplate reader (TECAN Sunrise, Tecan Trading AG, Switzerland). Blank wells (0.01–1 mg mL^{-1} NP without cells) were added to each set of experiments. All measurements were carried out in triplicate and each experiment was repeated at least twice.

Flow Cytometric Assays: All measurements were carried out on a CYTOMICS FC500 (Beckman Coulter Inc. Fullerton, CA), equipped with an argon laser (488 nm, 5 mV) and standard configuration with photomultiplier tube (PMT) fluorescence detector for green (525 nm, FL1), orange (575 nm, FL2), or red (610 nm, FL3) filtered light. After acquisition of at least 10 000 events per each run, data were stored as list mode files and analyzed with the FCS Express V3 software.

Flow Cytometric Assays—PI-Uptake Assay: For kinetic studies of membrane damage, cell suspensions (10^6 mL^{-1} cells per tube) in PBS were kept in a thermostated bath, to which was added the tested NP (0.01–1 mg mL^{-1}). For each time point (0, 5, 15, 30, and 60 min), aliquots of these treated cell suspensions were run in parallel to untreated controls, and Log FL3 for each sample obtained by flow cytometry, after adding 0.1 mg mL^{-1} PI solution, as indicated above.

Flow Cytometric Assays—Apoptosis Assay: JC-1 cyanine iodide (5,5′,6,6′-tetrachloro-1,1′,3,3′-tetraethyl-benzimidazolcarbocyanine iodide; Molecular Probes Europe BV, Leiden, The Netherlands), a mitochondrial inner membrane potential probe, was used as previously described.[82,85] Briefly, the probe (2.5 µg mL^{-1}) was added for 15 min to NP-treated or -untreated control cells, and then samples were washed twice, resuspended in PBS and immediately analyzed by flow cytometry, acquiring both LogFL2 and LogFL1 signals on viable cells (those excluding PI, run in parallel). JC-1 monomer was measured by the FL1-PMT, JC-1 aggregated by the FL2-PMT. Cells treated with 50×10^{-6} M of the uncoupler CCCP at 37 °C for 15 min were run in parallel as positive control (collapse of mitochondrial transmembrane potential).

Flow Cytometric Assays—NP Interaction with and Uptake into Cells: To a cell suspensions (10^6 mL^{-1} cells per tube) in PBS, kept in thermostated bath, were added BODIPY-labeled NPs at increasing concentrations (0.01, 0.1, 0.5, and 1 mg mL^{-1}) for increasing times (0, 5, 15, 30, and 60 min). Cells were run immediately or washed to remove unbound BODIPY-labeled NPs and run in parallel to untreated controls taken at the same time points on the flow cytometer. MFI values, obtained by the analysis of each single run, were normalized for each NP concentration to the MFI at the lowest concentration and shortest incubation time (5 min) to take into account differences in the intrinsic fluorescence of the particles.

Flow Cytometric Assays—Statistical Analysis: Data obtained from repeated experiments were subjected to computer-assisted analysis using GraphPad Instat 3, and statistical significance was assumed at $p \leq 0.05$ (ANOVA, Student–Newman–Keuls post test).

Confocal Microscopy: Cell suspensions (10^6 mL^{-1} cells per tube) were treated with M1- or M2-C8T/F8P/BODIPY AuNPs for 60 min in PBS, and subsequently washed twice at the end of the incubation time. Cells were then fixed (2% paraformaldehyde (PFA), 20 min), nuclei counterstained with Hoechst solution and cell sections were examined using a Nikon C1-SI confocal microscope (TE-2000U) equipped with a 20× and 60× oil immersion lens. Images were generated in the Optical Microscopy Center of the University of Trieste.

Atomic Force Microscopy—Chemicals: 18:1 (Δ9-Cis) DOPC, SM (Brain, Porcine), and cholesterol (ovine wool > 98%) were purchased by Avanti Polar Lipids (Alabaster, USA). Chloroform was provided by Fluka and Sigma Aldrich, (Milan, Italy).

Atomic Force Microscopy—Lipid Vesicles' Preparation and Supported Lipid Bilayer (SLB) Formation: SLB was prepared following the procedure described by Oropesa-Nuñez et al.,[86] with some modifications. The details are reported in the Supporting Information.

Atomic Force Microscopy—AFM Imaging: All AFM images were acquired using a commercially available microscope (MFP-3D Stand Alone AFM from Asylum Research, Santa Barbara, CA, USA). Measurements were carried out at room temperature working in dynamic tapping mode. For imaging, commercially available silicon cantilevers (OMCL-RC800PSA-1, Olympus Micro Cantilevers, nominal spring constant 0.76 N nm^{-1}) were chosen for imaging in liquid. Cantilevers were used working at low oscillation amplitudes with half-free amplitude set-point. High-resolution images (512 × 512 pixels frames) were acquired at 0.6÷1 lines s^{-1} scan speed.

Atomic Force Microscopy—AFM Data Analysis: AFM images were analyzed using Gwyddion, open-source modular program for scanning probe microscopy (SPM) data visualization and analysis.

Acknowledgements

D.M. and F.G. contributed equally to this work. The authors thank the Italian Ministry of University Research (MIUR) through the SIR project "Structure and FunctiOn at the Nanoparticle bioInterfAce"

(grant RBSI14PBC6) for financial support and the Swiss National Supercomputing Center for providing computational time. The authors are also grateful to the Optical Microscopy Center of the University of Trieste at the Life Sciences Department (www.units.it/confocal) for assistance in confocal microscopy acquisition and data analysis. The authors would like to thank Prof. Francesco Stellacci and Paolo Ronchese for support in MALDI-MS experiments and for scientific discussion. D.M. and S.B. performed molecular dynamics studies; M.S., P. Pengo, and E.P. contributed to the synthesis and characterization of the nanoparticles; F.G. performed SPR analysis; F.G., V.I., and S. Pacor performed cell toxicity, flow cytometry, and confocal microscopy experiments; F.P. and L.C. performed the AFM experiments; S. Polizzi performed the transmission electron microscopy (TEM) measurements; D.M., F.G., L.P., S. Pacor, A.T., and P. Posocco conceived the experimental design and contributed to the analysis of data; D.M., F.G., P. Pengo, L.P., S. Pacor, A.T., and P. Posocco wrote the manuscript; P. Posocco conceived the study.

Conflict of Interest

The authors declare no conflict of interest.

Keywords

fluorinated amphiphiles, Janus nanoparticles, membrane interaction, nano–bio interfaces, patterned surfaces

[1] S. E. A. Gratton, P. A. Ropp, P. D. Pohlhaus, J. C. Luft, V. J. Madden, M. E. Napier, J. M. De Simone, *Proc. Natl. Acad. Sci. USA* **2008**, *105*, 11613.
[2] C. D. Walkey, J. B. Olsen, H. Guo, A. Emili, W. C. W. Chan, *J. Am. Chem. Soc.* **2012**, *134*, 2139.
[3] A. Albanese, P. S. Tang, W. C. Chan, *Annu. Rev. Biomed. Eng.* **2012**, *14*, 1.
[4] E. Blanco, H. Shen, M. Ferrari, *Nat. Biotechnol.* **2015**, *33*, 941.
[5] S. Huo, Y. Jiang, A. Gupta, Z. Jiang, R. F. Landis, S. Hou, X.-J. Liang, V. M. Rotello, *ACS Nano* **2016**, *10*, 8732.
[6] S. G. Elci, Y. Jiang, B. Yan, S. T. Kim, K. Saha, D. F. Moyano, G. Yesilbag Tonga, L. C. Jackson, V. M. Rotello, R. W. Vachet, *ACS Nano* **2016**, *10*, 5536.
[7] D. F. Moyano, Y. Liu, D. Peer, V. M. Rotello, *Small* **2016**, *12*, 76.
[8] D. Marson, Y. Yang, S. Guldin, P. Posocco, in *Anisotropic Particle Assemblies* (Eds: N. Wu, D. Lee, A. Striolo), Elsevier, Amsterdam **2018**, p. 313.
[9] F. Manea, F. B. Houillon, L. Pasquato, P. Scrimin, *Angew. Chem., Int. Ed.* **2004**, *43*, 6165.
[10] P. Pengo, S. Polizzi, L. Pasquato, P. Scrimin, *J. Am. Chem. Soc.* **2005**, *127*, 1616.
[11] P. Pengo, L. Baltzer, L. Pasquato, P. Scrimin, *Angew. Chem., Int. Ed.* **2007**, *46*, 400.
[12] M. De, C.-C. You, S. Srivastava, V. M. Rotello, *J. Am. Chem. Soc.* **2007**, *129*, 10747.
[13] N. A. Kotov, *Science* **2010**, *330*, 188.
[14] M. Kopp, S. Kollenda, M. Epple, *Acc. Chem. Res.* **2017**, *50*, 1383.
[15] F. Schulz, G. T. Dahl, S. Besztejan, M. A. Schroer, F. Lehmkühler, G. Grübel, T. Vossmeyer, H. Lange, *Langmuir* **2016**, *32*, 7897.
[16] A. Centrone, E. Penzo, M. Sharma, J. W. Myerson, A. M. Jackson, N. Marzari, F. Stellacci, *Proc. Natl. Acad. Sci. USA* **2008**, *105*, 9886.
[17] J. J. Kuna, K. Voïtchovsky, C. Singh, H. Jiang, S. Mwenifumbo, P. K. Ghorai, M. M. Stevens, S. C. Glotzer, F. Stellacci, *Nat. Mater.* **2009**, *8*, 837.
[18] P. Pengo, M. Şologan, L. Pasquato, F. Guida, S. Pacor, A. Tossi, F. Stellacci, D. Marson, S. Boccardo, S. Pricl, P. Posocco, *Eur. Biophys. J.* **2017**, *46*, 749.
[19] A. Verma, O. Uzun, Y. Hu, Y. Hu, H. S. Han, N. Watson, S. Chen, D. J. Irvine, F. Stellacci, *Nat. Mater.* **2008**, *7*, 588.
[20] A. Hung, S. Mwenifumbo, M. Mager, J. J. Kuna, F. Stellacci, I. Yarovsky, M. M. Stevens, *J. Am. Chem. Soc.* **2011**, *133*, 1438.
[21] R. Huang, R. P. Carney, F. Stellacci, B. L. T. Lau, *Nanoscale* **2013**, *5*, 6928.
[22] A. Hung, M. Mager, M. Hembury, F. Stellacci, M. M. Stevens, I. Yarovsky, *Chem. Sci.* **2013**, *4*, 928.
[23] R. C. Van Lehn, P. U. Atukorale, R. P. Carney, Y. S. Yang, F. Stellacci, D. J. Irvine, A. Alexander-Katz, *Nano Lett.* **2013**, *13*, 4060.
[24] R. Huang, R. P. Carney, K. Ikuma, F. Stellacci, B. L. T. Lau, *ACS Nano* **2014**, *8*, 5402.
[25] R. C. Van Lehn, M. Ricci, P. H. J. Silva, P. Andreozzi, J. Reguera, K. Voitchovsky, F. Stellacci, A. Alexander-Katz, *Nat. Commun.* **2014**, *5*, 4482.
[26] P. U. Atukorale, Y. S. Yang, A. Bekdemir, R. P. Carney, P. J. Silva, N. Watson, F. Stellacci, D. J. Irvine, *Nanoscale* **2015**, *7*, 11420.
[27] S. Sabella, R. P. Carney, V. Brunetti, M. A. Malvindi, N. Al-Juffali, G. Vecchio, S. M. Janes, O. M. Bakr, R. Cingolani, F. Stellacci, P. P. Pompa, *Nanoscale* **2014**, *6*, 7052.
[28] G. Rossi, L. Monticelli, *Biochim. Biophys. Acta, Biomembr.* **2016**, *1858*, 2380.
[29] T. Kunitake, S. Tawaki, N. Nakashima, *Bull. Chem. Soc. Jpn.* **1983**, *56*, 3235.
[30] R. Elbert, T. Folda, H. Ringsdorf, *J. Am. Chem. Soc.* **1984**, *106*, 7687.
[31] M. Şologan, M. Boccalon, S. Bidoggia, C. Gentilini, L. Pasquato, P. Pengo, *Supramol. Chem.* **2017**, *29*, 808.
[32] M. P. Krafft, *Adv. Drug Delivery Rev.* **2001**, *47*, 209.
[33] J. G. Riess, *Curr. Opin. Colloid Interface Sci.* **2009**, *14*, 294.
[34] Z. Zhang, W. Shen, J. Ling, Y. Yan, J. Hu, Y. Cheng, *Nat. Commun.* **2018**, *9*, 1377.
[35] L. Dafik, V. Kalsani, A. K. L. Leung, K. Kumar, *J. Am. Chem. Soc.* **2009**, *131*, 12091.
[36] M. C. Z. Kasuya, S. Nakano, R. Katayama, K. Hatanaka, *J. Fluorine Chem.* **2011**, *132*, 202.
[37] M. Carril, D. Padro, P. del Pino, C. Carrillo-Carrion, M. Gallego, W. J. Parak, *Nat. Commun.* **2017**, *8*, 1542.
[38] M. E. Kurczy, Z.-J. Zhu, J. Ivanisevic, A. M. Schuyler, K. Lalwani, A. F. Santidrian, J. M. David, A. Giddabasappa, A. J. Roberts, H. J. Olivos, P. J. O'Brien, L. Franco, M. W. Fields, L. P. Paris, M. Friedlander, C. H. Johnson, A. A. Epstein, H. E. Gendelman, M. R. Wood, B. H. Felding, G. J. Patti, M. E. Spilker, G. Siuzdak, *Nat. Commun.* **2015**, *6*, 5998.
[39] M. Boccalon, P. Franchi, M. Lucarini, J. J. Delgado, F. Sousa, F. Stellacci, I. Zucca, A. Scotti, R. Spreafico, P. Pengo, L. Pasquato, *Chem. Commun.* **2013**, *49*, 8794.
[40] O. Michelena, D. Padro, C. Carrillo-Carrión, P. del Pino, J. Blanco, B. Arnaiz, W. J. Parak, M. Carril, *Chem. Commun.* **2017**, *53*, 2447.
[41] P. Posocco, C. Gentilini, S. Bidoggia, A. Pace, P. Franchi, M. Lucarini, M. Fermeglia, S. Pricl, L. Pasquato, *ACS Nano* **2012**, *6*, 7243.
[42] G. Cavallo, P. Metrangolo, R. Milani, T. Pilati, A. Priimagi, G. Resnati, G. Terraneo, *Chem. Rev.* **2016**, *116*, 2478.
[43] C. Gentilini, P. Franchi, E. Mileo, S. Polizzi, M. Lucarini, L. Pasquato, *Angew. Chem., Int. Ed.* **2009**, *48*, 3060.

[44] F. Biscarini, Q. K. Ong, C. Albonetti, F. Liscio, M. Longobardi, K. S. Mali, A. Ciesielski, J. Reguera, C. Renner, S. De Feyter, P. Samorì, F. Stellacci, *Langmuir* **2013**, *29*, 13723.
[45] M. Şologan, D. Marson, S. Polizzi, P. Pengo, S. Boccardo, S. Pricl, P. Posocco, L. Pasquato, *ACS Nano* **2016**, *10*, 9316.
[46] X. Liu, M. Yu, H. Kim, M. Mameli, F. Stellacci, *Nat. Commun.* **2012**, *3*, 1182.
[47] J. Reguera, *J. Phys. Chem. C* **2018**, *122*, 20871.
[48] K. M. Harkness, A. Balinski, J. A. McLean, D. E. Cliffel, *Angew. Chem., Int. Ed.* **2011**, *50*, 10554.
[49] P. Ronchese, P. Pengo, F. Stellacci, L. Pasquato, *Unpublished*.
[50] Z. Luo, D. Marson, Q. K. Ong, A. Loiudice, J. Kohlbrecher, A. Radulescu, A. Krause-Heuer, T. Darwish, S. Balog, R. Buonsanti, D. I. Svergun, P. Posocco, F. Stellacci, *Nat. Commun.* **2018**, *9*, 1343.
[51] S. Zhang, A. Nelson, P. A. Beales, *Langmuir* **2012**, *28*, 12831.
[52] R. C. Van Lehn, P. U. Atukorale, R. P. Carney, Y.-S. Yang, F. Stellacci, D. J. Irvine, A. Alexander-Katz, *Nano Lett.* **2013**, *13*, 4060.
[53] J. M. Troiano, L. L. Olenick, T. R. Kuech, E. S. Melby, D. Hu, S. E. Lohse, A. C. Mensch, M. Dogangun, A. M. Vartanian, M. D. Torelli, E. Ehimiaghe, S. R. Walter, L. Fu, C. R. Anderton, Z. Zhu, H. Wang, G. Orr, C. J. Murphy, R. J. Hamers, J. A. Pedersen, F. M. Geiger, *J. Phys. Chem. C* **2015**, *119*, 534.
[54] E. S. Melby, A. C. Mensch, S. E. Lohse, D. Hu, G. Orr, C. J. Murphy, R. J. Hamers, J. A. Pedersen, *Environ. Sci.: Nano* **2016**, *3*, 45.
[55] E. Rascol, J.-M. Devoisselle, J. Chopineau, *Nanoscale* **2016**, *8*, 4780.
[56] The reduced ΔG_{adh} of mixed NPs could be due, at least in part, to the overall lower number of ligands with respect to homoligand NPs, resulting in fewer contacts. For this reason, computational runs with mixed ligand NPs constructed to have the same number of ligands (≈70) and diameter (≈2 nm) of homoligand NPs were carried out, but continued to show a reduced N_C (data not shown), so that the presence of a mixed system results in reduced contacts.
[57] D. Lingwood, K. Simons, *Science* **2010**, *327*, 46.
[58] J. H. Lorent, B. Diaz-Rohrer, X. Lin, K. Spring, A. A. Gorfe, K. R. Levental, I. Levental, *Nat. Commun.* **2017**, *8*, 1219.
[59] E. Sezgin, I. Levental, S. Mayor, C. Eggeling, *Nat. Rev. Mol. Cell Biol.* **2017**, *18*, 361.
[60] T. Fischer, H. Jelger Risselada, R. L. C. Vink, *Phys. Chem. Chem. Phys.* **2012**, *14*, 14500.
[61] X. Chen, D. P. Tieleman, Q. Liang, *Nanoscale* **2018**, *10*, 2481.
[62] T. Róg, M. Pasenkiewicz-Gierula, I. Vattulainen, M. Karttunen, *Biochim. Biophys. Acta, Biomembr.* **2009**, *1788*, 97.
[63] W. K. Subczynski, M. Pasenkiewicz-Gierula, J. Widomska, L. Mainali, M. Raguz, *Cell Biochem. Biophys.* **2017**, *75*, 369.
[64] An attempt was also made to assess cell damage in terms of decreased mitochondrial functionality by measuring NP effect on the inner transmembrane potential ($\Delta\psi_m$), using the DiOC6 probe. This dye is a selective $\Delta\psi_m$ probe often employed as a marker of early apoptotic events, as it loses fluorescence on mitochondrial inner membrane depolarization. However, it proved inappropriate for our studies as both M1- and M2-C8T/F8P AuNPs quenched its fluorescence in vitro (likely due to the absorbance by the Au core) even in the absence of cells.
[65] D. Wlodkowic, W. Telford, J. Skommer, Z. Darzynkiewicz, in *Methods in Cell Biology* (Eds: Z. Darzynkiewicz, E. Holden, A. Orfao, W. Telford, D. Wlodkowic), Vol. *103*, Academic Press, San Diego, CA **2011**, p. 55.
[66] *Biacore—Sensor Surface Handbook, BR-1005-71*, GE Healthcare Bio-Sciences AB, Uppsala, Sweden **2005**.
[67] G. Anderluh, M. Beseničar, A. Kladnik, J. H. Lakey, P. Maček, *Anal. Biochem.* **2005**, *344*, 43.
[68] M. Beseničar, P. Maček, J. H. Lakey, G. Anderluh, *Chem. Phys. Lipids* **2006**, *141*, 169.
[69] D. A. Case, V. Babin, J. T. Berryman, R. M. Betz, Q. Cai, D. S. Cerutti, T. E. Cheatham, T. A. I. Darden, R. E. Duke, H. Gohlke, A. W. Goetz, S. Gusarov, N. Homeyer, P. Janowski, J. Kaus, I. Kolossváry, A. Kovalenko, T. S. Lee, S. LeGrand, T. Luchko, R. Luo, B. Madej, K. M. Merz, F. Paesani, D. R. Roe, A. Roitberg, C. Sagui, R. Salomon-Ferrer, G. Seabra, C. L. Simmerling, W. Smith, J. Swails, R. C. Walker, J. Wang, R. M. Wolf, X. Wu, P. A. Kollman, *AMBER 14*, University of California, San Francisco, CA **2014**.
[70] J. Wang, W. Wang, P. A. Kollman, D. A. Case, *J. Mol. Graph. Model.* **2006**, *25*, 247.
[71] J. Wang, R. M. Wolf, J. W. Caldwell, P. A. Kollman, D. A. Case, *J. Comput. Chem.* **2004**, *25*, 1157.
[72] S. J. Marrink, H. J. Risselada, S. Yefimov, D. P. Tieleman, A. H. de Vries, *J. Phys. Chem. B* **2007**, *111*, 7812.
[73] M. J. Abraham, T. Murtola, R. Schulz, S. Páll, J. C. Smith, B. Hess, E. Lindahl, *SoftwareX* **2015**, *1–2*, 19.
[74] H. J. C. Berendsen, D. van der Spoel, R. van Drunen, *Comput. Phys. Commun.* **1995**, *91*, 43.
[75] D. Van Der Spoel, E. Lindahl, B. Hess, G. Groenhof, A. E. Mark, H. J. C. Berendsen, *J. Comput. Chem.* **2005**, *26*, 1701.
[76] B. Hess, C. Kutzner, D. van der Spoel, E. Lindahl, *J. Chem. Theory Comput.* **2008**, *4*, 435.
[77] S. Pronk, S. Páll, R. Schulz, P. Larsson, P. Bjelkmar, R. Apostolov, M. R. Shirts, J. C. Smith, P. M. Kasson, D. van der Spoel, B. Hess, E. Lindahl, *Bioinformatics* **2013**, *29*, 845.
[78] P. Szilárd, M. J. Abraham, C. Kutzner, B. Hess, E. Lindahl, *Proc. EASC* **2014**, *8759*, 3.
[79] S. Kumar, J. M. Rosenberg, D. Bouzida, R. H. Swendsen, P. A. Kollman, *J. Comput. Chem.* **1992**, *13*, 1011.
[80] W. Humphrey, A. Dalke, K. Schulten, *J. Mol. Graph.* **1996**, *14*, 33.
[81] T. A. Wassenaar, H. I. Ingólfsson, R. A. Böckmann, D. P. Tieleman, S. J. Marrink, *J. Chem. Theory Comput.* **2015**, *11*, 2144.
[82] S. Pacor, A. Grillo, L. Dordević, S. Zorzet, M. Lucafò, T. Da Ros, M. Prato, G. Sava, *Biomed Res. Int.* **2015**, *2015*, 1.
[83] A. Kroll, M. H. Pillukat, D. Hahn, J. Schnekenburger, *Eur. J. Pharm. Biopharm.* **2009**, *72*, 370.
[84] N. A. Monteiro-Riviere, A. O. Inman, L. W. Zhang, *Toxicol. Appl. Pharmacol.* **2009**, *234*, 222.
[85] A. Cossarizza, S. Salvioli, *Current Protocols in Cytometry*, John Wiley & Sons, Inc., New York, NY **2000**, p. 9.14.1.
[86] R. Oropesa-Nunez, S. Seghezza, S. Dante, A. Diaspro, R. Cascella, C. Cecchi, M. Stefani, F. Chiti, C. Canale, *Oncotarget* **2016**, *7*, 44991.